ENHANCED PHOTODEGRADATION OF 2,4-DICHLOROPHENOXYACETIC ACID BY THE HETEROJUNCTION OF TiO_2 AND Fe-MCM 41 MATERIAL

QUANG PHÂN HỦY 2,4- DICHLOROPHENOXYACETIC ACID TRÊN VẬT LIỆU DỊ THỂ TiO_2 VÀ Fe-MCM 41

Phung Thi Lan[1,*], Nguyen Thi Oanh[1], Dang Dinh Anh Tuan[2], Nguyen Thi Kim Giang[1]

DOI: http://doi.org/10.57001/huih5804.2025.165

ABSTRACT

The aim of this study was to synthesize the TiO_2/Fe-MCM-41 heterojunction material using the ultrasonic method for the photodegradation of 2,4-dichlorophenoxyacetic acid (2,4-D) under light irradiation. The synthesized materials were characterized using various techniques, including XRD, FE-SEM, UV-Vis DRS, and EDX. These analyses confirmed that TiO_2 particles were uniformly dispersed on the Fe-MCM-41 support. The integration of TiO_2 with Fe-MCM-41 enhanced visible light absorption, which in turn improved photocatalytic activity under light irradiation. Among the tested conditions, the optimal performance was observed with a TiO_2 loading of 30% (corresponding to a mass-to-volume ratio of 0.5g/L), an initial 2,4-D concentration of 40ppm, a pH of 4.2, and an illumination time of 210 minutes. Under these conditions, the photodegradation efficiency exceeded 97%. Additionally, radical scavenging experiments indicated that superoxide radicals ($O_2^{\bullet -}$), hydroxyl radicals (•OH), and photogenerated holes (h^+) played critical roles in the photocatalytic degradation process. The TiO_2/Fe-MCM-41 catalyst also demonstrated stable performance over four consecutive cycles, highlighting its potential for repeated use in photocatalytic applications.

Keywords: *TiO_2; Fe-MCM41; photocatalysis, mechanism.*

TÓM TẮT

Vật liệu TiO_2/Fe-MCM-41 được nghiên cứu tổng hợp cho quá trình quang phân hủy 2,4-D dưới điều kiện chiếu sáng. Các kết quả phân tích về phổ XRD, FE-SEM, UV-Vis DRS và EDX, cho thấy TiO_2 phân tán đều trên Fe-MCM-41 và sự kết hợp dị thể giữa hai thành phần đã tăng khả năng hấp thụ ánh sáng và cải thiện hoạt tính quang xúc tác. Hiệu suất phân hủy 2,4-D đạt trên 97% đối với vật liệu 30%TiO_2/Fe-MCM-41 ở điều kiện thực nghiệm: nồng độ ban đầu 2,4-D là 40ppm, pH 4,2, tỷ lệ khối lượng chất xúc tác và thể tích dung dịch là 0,5g/L, thời gian chiếu sáng 210 phút chiếu sáng. Các gốc $O_2^{\bullet -}$, $^{\bullet}OH$ và h^+ đóng vai trò chính trong quá trình phản ứng. Vật liệu cho thấy độ ổn định cao sau 4 chu kỳ sử dụng.

Từ khoá: *TiO_2; Fe-MCM 41; quá trình quang xúc tác; cơ chế.*

[1]Faculty of Chemistry, Hanoi National University of Education, Vietnam

[2]Specialized in Physics, High School for Gifted Students, Hanoi National University of Education, Vietnam

[*]Email: lanpt@hnue.edu.vn

Received: 19/2/2025

Revised: 21/5/2025

Accepted: 28/5/2025

1. INTRODUCTION

Advanced oxidation processes (AOPs) have emerged as effective treatment technologies for addressing persistent organic pollutants that are resistant to biodegradation. These processes are characterized by the generation of highly reactive species, including hydroxyl radicals ($^{\bullet}OH$), superoxide radicals ($O_2^{\bullet -}$), and photogenerated holes (h^+), which play a key role in the

degradation of these pollutants. Numerous semiconductors have been investigated for their potential applications as photocatalysts, including TiO_2 [1, 2], $BiVO_4$ [3], MoS_2[4], g-C_3N_4 [5], etc. Among these semiconductors, TiO_2 has become a promising material and is widely used in photocatalytic processes due to its outstanding properties, such as high optical and electronic properties, high photocatalytic activity, high chemical stability, low cost, non-toxicity, and being environmentally friendly. Nevertheless, TiO_2 has a band gap energy of nearly 3.2eV, in which the valence band energy is 2.9eV and the conduction band energy is about - 0.3eV, only absorbing light well in the ultraviolet region (UV, $\lambda < 380$nm). Furthermore, TiO_2 readily aggregates in suspension due to its small size, which results in a decrease in catalytic activity and effective surface area. In addition, using these tiny particles means paying a lot of money for filtration in order to get rid of the catalyst when the reaction is complete. In order to overcome these restrictions, TiO_2 is modified with some other semiconductors [6, 7] and porous materials [8, 9] to improve its ability to absorb light, especially by expanding the light absorption region at longer wavelengths ($\lambda > 400$nm) to lower the photogenerated electron-hole recombination rate and band gap energy.

Among porous materials, silica mesoporous materials [8, 10, 11] have been receiving great attention due to their large specific surface area, controlled capillary system, and size distribution, narrow capillary size, highly ordered hexagonal structure, contains a silanol functional group, so it can act as both an adsorbent material and a carrier to disperse catalytic sites as well as fine connectivity of the pores facilitating the transfer of organic substrates. Accordingly, it contributes to improving the elimination of pollutants through photodegradation. In a review of some recent investigations, MCM 41, a silica mesoporous material, has improved photocatalytic activity of TiO_2. Studies have shown that enhanced photocatalytic activity is mainly due to the synergy effects of the high surface area of MCM-41, well-distributed TiO_2, and reduced electron-hole recombination rates. Furthermore, a hexagonal packed array of channels in the typical structure of these mesoporous materials facilitates a high photocatalytic active species dispersion [12 -14]. Therefore, it might be possible to create a photocatalyst being activated with visible radiation and with easy recovery from the aqueous suspensions.

In this study, TiO_2 particles synthesizing by hydrolysis method were deposited on the surface of the Fe-MCM-41 material by ultrasound method to improve the dispersion of TiO_2, and the as-synthesized TiO_2/Fe-MCM-41 composites were used as a photocatalyst for the oxidation of 2, 4-dichlorophenol acetic acid (2,4-D) under both UV and visible light irradiation. According to the results of the project coded DTĐL.CN-66/19 conducted by the Ministry of Industry and Trade from 2019 to 2022, led by Associate Professor Dr. Le Minh Cam, residues of 2,4-D -a highly persistent environmental pollutant - still remain in the soil in certain areas of Nghe An, due to its use prior to 2017. These residues continue to affect the quality of both soil and water in the region. Therefore, it is necessary to continue treating 2,4-D contamination to protect environmental quality, even in areas where residues are no longer present, as a precautionary measure.

2. MATERIALS AND METHODS

2.1. Synthesis of material

Procedure for synthesizing TiO_2

Pristine TiO_2 was synthesized via a hydrolysis method as follows: 5mL of $TiCl_4$ was added to 30mL of ethanol pre-cooled in ice water for 30 minutes, followed by vigorous stirring for 6 hours. The mixture's pH was then adjusted to 7 using NH_3 solution and stirred at 60°C until a white gel formed. The gel was aged at room temperature for 18 hours, dried at 80°C overnight, and annealed sequentially at 300°C (1h), 400°C (1h), and 550°C (3h).

Procedure for preparing Fe-MCM 41

Fe-MCM-41 was synthesized in two steps. First, MCM-41 sample was prepared by dissolving 2.4g CTAB (Cetrimonium bromide) in 120mL distilled water, followed by the addition of 8mL NH_3 and 10mL TEOS (Tetraethyl orthosilicate) with vigorous stirring for 12 hours. The resulting solid was filtered, washed with water and ethanol, then annealed at 550°C for 5 hours. In the second step, 0.05g $FeSO_4{\cdot}7H_2O$ (in 10mL water) was mixed with 0.5g MCM-41 (in 10mL ethanol) and stirred for 3 hours to dope Fe into MCM-41. The solid was filtered, washed with ethanol, dried overnight at room temperature, and annealed at 550°C for 4 hours.

Procedure for preparing TiO2/Fe-MCM 41

TiO_2/Fe-MCM-41 was synthesized using an ultrasonic method (30kHz). For 30% TiO_2 loading, 0.3g of Fe-MCM-41 and 0.129g of TiO_2 were dispersed in 30mL of ethanol and sonicated at ~35°C for 90 minutes using an on/off cycle. The mixture was then filtered and dried at 80°C overnight. For 45% TiO_2/Fe-MCM-41, 0.245g of TiO_2 was used, following the same procedure.

2.2. Characterization techniques

Characterization was conducted as follows: XRD pattern (X-ray diffraction) was carried on a Bruker D8 Advance with Cu-Kα radiation (λ = 0.15418nm) to identify crystalline phases; EDX spectra (Energy-dispersive X-ray spectroscopy) and FESEM image (Field emission scanning electron microscopy) was performed on a FESEM S-4800 to analyze elemental composition and morphology; and UV-Vis DRS spectra (Ultraviolet-visible diffuse reflectance spectroscopy) was carried on a Shimadzu UV-2600 to assess optical properties.

Experiment with 2,4-D photocatalytic activity

The photocatalytic activity of the synthesized catalysts was evaluated using 2,4-D (40 ppm, pH 4.2) as a model pollutant. In each test, 75mg of catalyst and 150mL of 2,4-D solution (0.5g/L) were added to the quartz glass beaker placed in a temperature-controlled bath at 25°C. Then, the mixture was stirred continuously and irradiated with a 250W xenon lamp equipped with a UV cut-off filter (λ > 400nm) positioned 20cm above the solution. Prior to illumination, all samples underwent a 60-minute dark adsorption period to reach adsorption - desorption equilibrium. The concentration of 2,4-D was determined using a standard curve equation that describes the relationship between absorbance and concentration at a wavelength of 283nm, based on ultra-visible absorption spectroscopy. The equation used was: A = 0.0085*C + 0.0059, R^2 = 0.998 where C represents the concentration of 2,4-D, and A is the absorbance at 283nm. In this study, the decomposition of 2,4-D was also investigated under conditions using only a 250W lamp for illumination and without the use of a catalyst. Under these conditions, the decomposition efficiency was very low, measuring below 3% (Fig. 6). This suggests that 2,4-D was barely decomposed, and only a negligible amount may have evaporated though this could not be confirmed due to the inability to determine the experimental measurement error. To ensure safety during the experiment, an exhaust fan system was installed near the testing area.

3. RESULTS AND DISCUSSION

3.1. Characterization

The crystal structure of the samples was evaluated through XRD pattern. Fig. 1 displayed the XRD pattern of Fe-MCM 41, TiO_2, 30%TiO_2/Fe-MCM 41, and 45%TiO_2/Fe-MCM 41.

As seen in Fig. 1, a diffraction peak at a narrow angle 2θ of 2.4° on the XRD pattern of Fe-MCM 41 material is observed, which is characteristic of the (100) plane and can be indexed to a hexagonal lattice, demonstrating the mesoporous structure of MCM 41 material [13 -16]. For TiO_2 material, characteristic diffraction peaks with the greatest intensity can be observed at the angle 2θ of 25.3° corresponding to the reflection plane (101), and other characteristic peaks with low intensity at the angle 2θ of 37.98°, 48.08°, 53.8°, 55.04°, 62.60° which characterized the plane (004), (200), (105), (211), and (204). This result was quite consistent with previous publications. The strong peak at the angles 2θ = 25.3° and 48.08° indicated that the synthesized TiO_2 exists mainly in anatase form (JCPDS Card No. 00 021 1272) [13, 22].

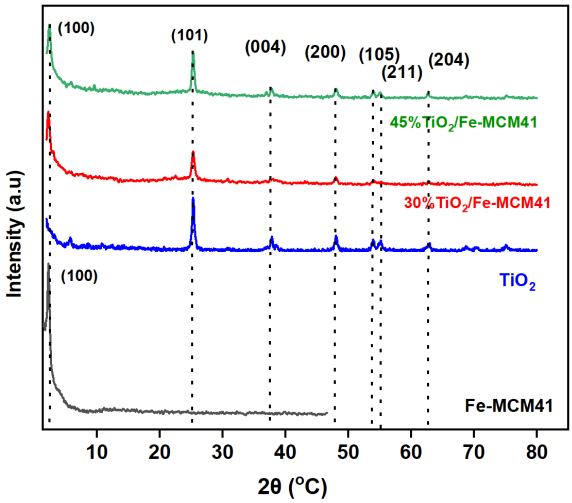

Fig. 1. XRD pattern of Fe-MCM41, TiO_2, 30%TiO_2/Fe-MCM41, and 45%TiO_2/Fe-MCM41

In the XRD patterns of 30% and 45% TiO_2/Fe-MCM-41, characteristic peaks of both TiO_2 and Fe-MCM-41 are present. As TiO_2 loading increased from 30% to 45%, TiO_2 peak intensities became stronger, while Fe-MCM-41 peaks weakened slightly, indicating a strong interaction between the two components. This observation is consistent with previous studies [14 -16].

The average crystallite sizes of as-synthesized material have been determined by using the Debye-Scherer formula [17]:

$$D = \frac{K.\lambda}{\beta.\cos\theta} = \frac{0.9*\lambda}{B.\cos\theta} \quad (1)$$

Where, K being the crystallite shape factor, λ the X-ray wavelength (1.5406 nm for Cu K), B, β is Half-width at maximum diffraction peak and θ is the Bragg angle.

The crystallite sizes of TiO_2, 30% TiO_2/Fe-MCM-41, and 45% TiO_2 /Fe-MCM-41 were calculated using the (101) plane at 2θ ≈ 25.3°. The average sizes were 20.31nm, 18.03nm, and 18.75nm, respectively. These results indicate that incorporating TiO_2 into the Fe-MCM-41

matrix reduces its crystallite size, although increasing the TiO_2 loading from 30% to 45% slightly increases the particle size.

The morphology of the as-synthesized samples was evaluated through FESEM images shown in Fig. 2.

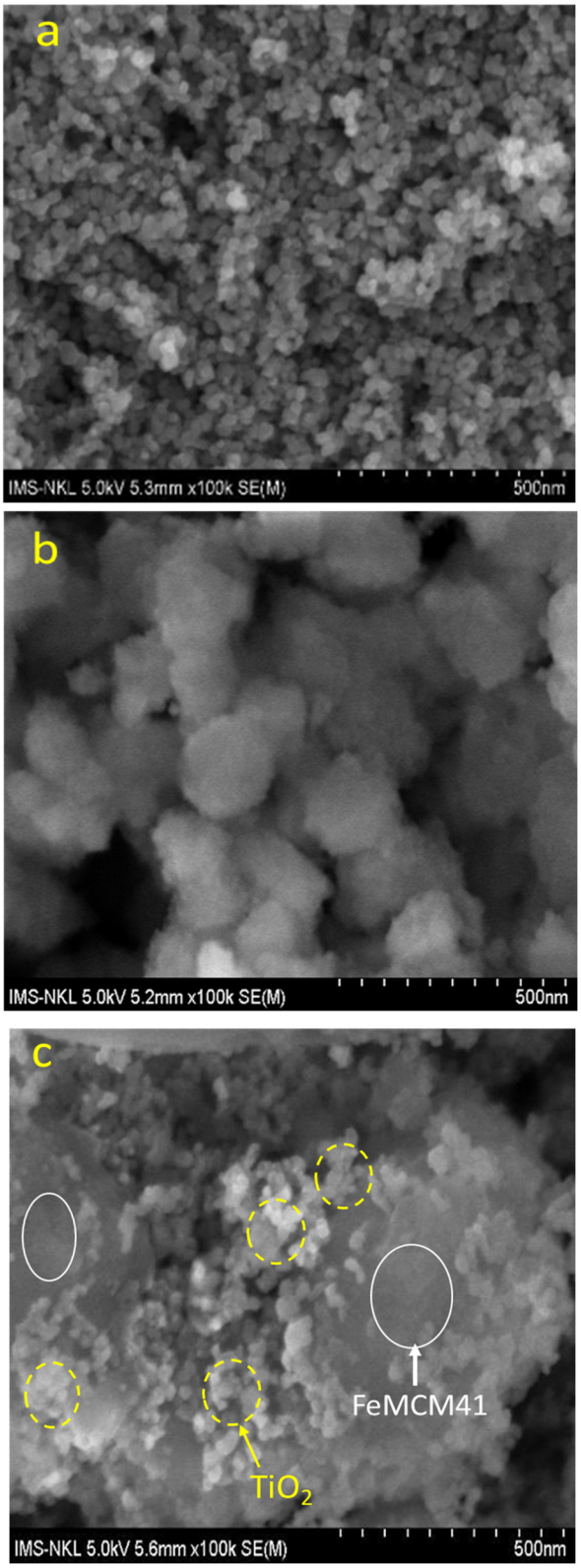

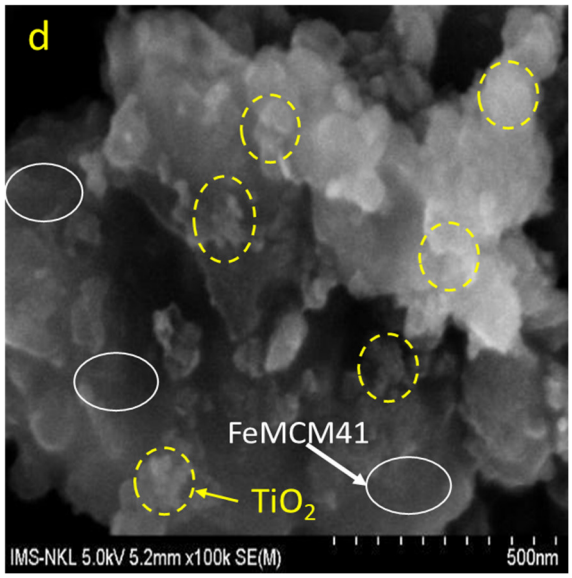

Fig. 2. FE-SEM images of (a) TiO_2, (b) Fe-MCM 41, (c) 30%TiO_2/Fe-MCM 41 and (d) 45%TiO_2/Fe-MCM 41

As shown in Fig. 2a and 2b, both TiO_2 and Fe-MCM-41 particles exhibit uniform, near-spherical shapes. In the composites (Fig. 2c and 2d), TiO_2 particles are embedded within the Fe-MCM-41 structure and form small clusters. At 30% TiO_2 loading, the distribution is more uniform, with less shrinkage compared to the 45%TiO_2 loading. Ultrasonic treatment effectively facilitated the even attachment of TiO_2 onto the Fe-MCM-41 surface, suggesting the formation of a heterojunction that may enhance electron-hole separation and photocatalytic performance. Particle sizes determined from FESEM images showed that pure TiO_2 ranged from 20 - 30nm, while 30% TiO_2/Fe-MCM-41 remained similar at 23 - 30nm. However, with 45% TiO_2 loading, particle size increased significantly to 50 - 80 nm, consistent with the trend observed in crystallite size analysis.

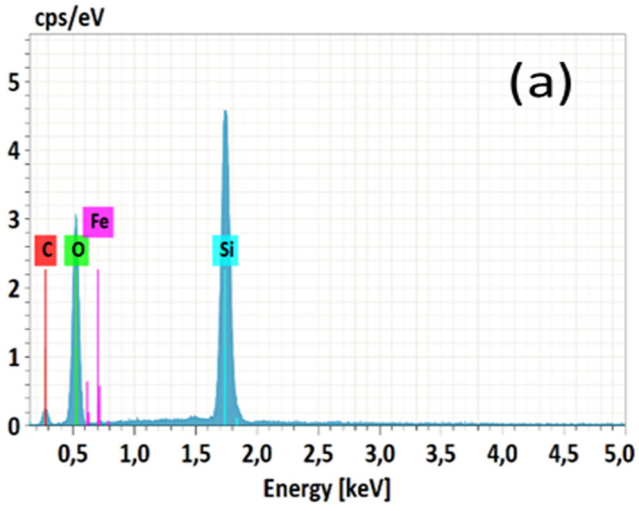

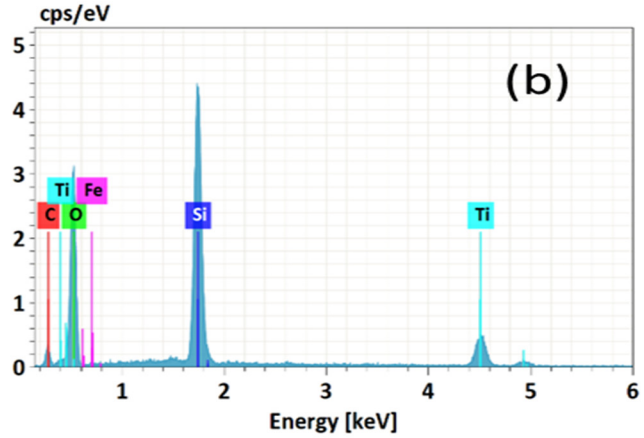

Fig. 3. EDX spectra of (a) Fe-MCM41 and (b) 30%TiO2/Fe-MCM41

Table 1. Chemical elemental compositions from EDX spectra (wt%)

Samples	C	Si	O	Fe	Ti	Total (%)
Fe-MCM41	14.91	28.64	55.60	0.85	0.00	100.00
30%TiO_2-Fe-MCM41	13.31	24.29	46.90	1.00	14.50	100.00

EDX spectra were examined for Fe-MCM-41 and 30% TiO_2/Fe-MCM-41 samples, with elemental compositions calculated based on the reaction equations. The results are shown in Fig. 3 and summarized in Table 1.

The EDX spectra confirmed the presence of C, O, Si, and Fe in both Fe-MCM-41 and 30%TiO_2/Fe-MCM-41 samples. In the composite, Ti was also detected with a weight percentage of approximately 14.5%, indicating mixture of TiO_2 and Fe-MCM-41.

The optical properties of the samples were evaluated using UV vis DRS spectra. As shown in Fig. 4, the UV-Vis DRS spectra of TiO_2, Fe-MCM-41, 30% TiO_2/Fe-MCM-41, and 45% TiO_2/Fe-MCM-41 were recorded over the wavelength range of 200 - 800nm.

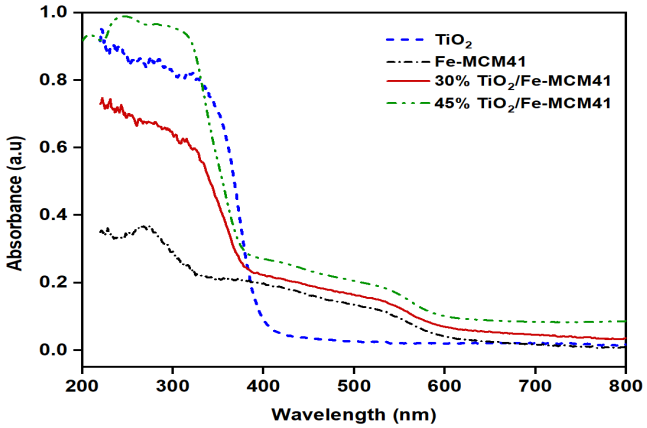

Fig. 4. UV-Vis DRS of TiO_2, Fe-MCM 41, 30%TiO_2/Fe-MCM 41, and 45%TiO_2/Fe-MCM 41

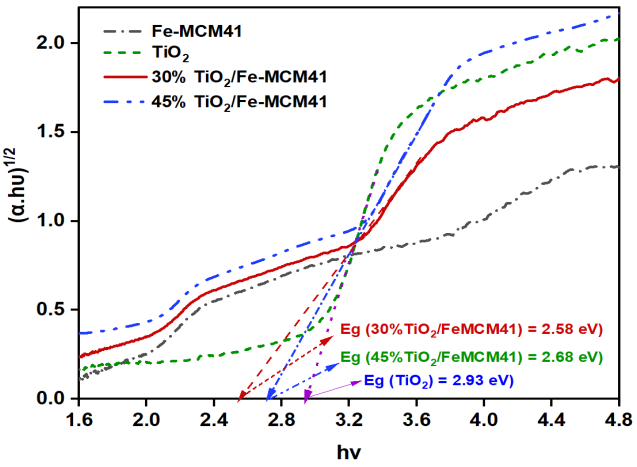

Fig. 5. The Tauc plots $((\alpha h\nu)^{1/2}$ vs. hν of TiO_2, Fe-MCM 41, 30%TiO_2/Fe-MCM 41, and 45%TiO_2/Fe-MCM 41

As shown in Fig. 4, TiO_2 exhibits strong UV light absorption with an absorption edge at 380nm, while Fe-MCM-41 absorbs light in both the UV and visible regions. The composites (30% and 45% TiO_2/Fe-MCM-41) show enhanced visible light absorption, attributed to the broad absorption of Fe-MCM-41. This improved light absorption contributes to enhanced photocatalytic activity under light irradiation.

Additionally, the Tauc theory (Eq. (2)) was used to determine the energy band gap (E_g) values of the studied samples [18]:

$$(\alpha.h\upsilon)^{n} = A(h\upsilon - E_g) \quad (2)$$

Where α is the optical absorption intensity (a.u), h is the Planck's constant (h = 6.625 x 10^{-34}J.s), ν is the frequency of the incident radiation (ν = c/λ, where c is the speed of light and λ is the wavelength), n = ½ and A is a proportionality constant.

Fig. 5 shows the Tauc plots $((\alpha h\nu)^{1/2}$ vs. hν) for TiO_2, 30% TiO_2/Fe-MCM-41, and 45% TiO_2/Fe-MCM-41. The calculated band gap energies were 2.93eV for TiO_2, 2.58eV for 30% TiO_2/Fe-MCM-41, and 2.68eV for 45%TiO_2/Fe-MCM-41. The reduced band gaps in the composites indicate enhanced visible light absorption, likely due to the formation of a TiO_2/Fe-MCM-41 heterojunction. This extended absorption into the visible range contributes to improved photocatalytic performance under light irradiation.

3.2. Photocatalytic activity of TiO2/Fe-MCM 41 for 2,4-D removal

Effect of TiO_2 loading

Fig. 6 presents the 2,4-D removal efficiency for TiO_2, Fe-MCM-41, 30% TiO_2/Fe-MCM-41, and 45% TiO_2/Fe-

MCM-41. For comparison, photodegradation was also tested without a catalyst under the same light conditions. Prior to illumination, all samples underwent a 60-minute dark adsorption period to reach adsorption-desorption equilibrium. The results showed negligible adsorption of 2,4-D in the dark, indicating that removal was primarily due to photocatalytic activity.

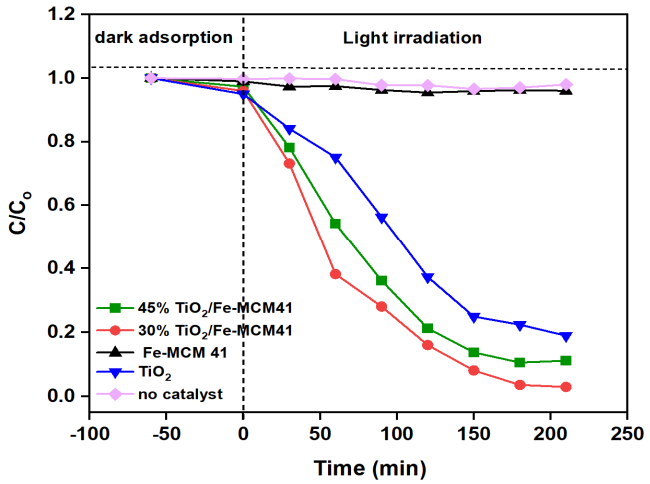

Fig. 6. The degradation efficiency vs. irradiation time over as-synthesized catalysts

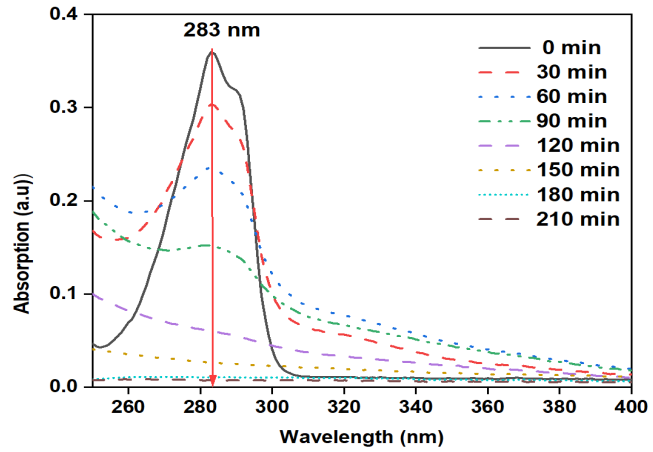

Fig. 7. UV Vis spectra of 2,4-D solution under illumination over 30%TiO$_2$/Fe-MCM 41 material

The results showed that in the absence of a catalyst, illumination with a 250W xenon lamp had little effect on 2,4-D degradation. Fe-MCM-41 also displayed very low photocatalytic activity, achieving only about 4% degradation. In Fig. 6, the "no catalyst" line and the "Fe-MCM-41" line exhibit similar trends and are closely aligned, indicating that Fe-MCM-41 alone has no significant catalytic activity. Instead, Fe-MCM-41 functions as a catalyst support, aiding in the reduction of the recombination rate of photogenerated electrons and holes when combined with TiO_2. In contrast, pure TiO_2 degraded approximately 43.69% of 2,4-D after 90 minutes, with the degradation increasing to 81.07% after 210 minutes. Notably, the 30%TiO_2/Fe-MCM-41 composite demonstrated even higher photocatalytic efficiency than pure TiO_2 under the same conditions.

The 30%TiO_2/Fe-MCM-41 composite achieved 71.97% 2,4-D degradation after 90 minutes and 97.01% after 210 minutes of illumination. UV-Vis DRS analysis confirmed that coupling TiO_2 with Fe-MCM-41 reduced the band gap and enhanced visible light absorption, improving photocatalytic performance. This enhancement is also attributed to efficient charge separation, as electrons quickly transfer from TiO_2 to the electron-rich Fe-MCM-41 matrix, reducing recombination. However, increasing TiO_2 content to 45% slightly reduced efficiency, likely due to the formation of larger TiO_2 clusters, which hinder light absorption and limit electron-hole pair generation. From the Fig. 7, it can be seen that the peak specific to 2,4-D at 283nm were clearly decreased with increasing illumination time and this peak disappeared at 210 min of illumination time.

Effect of the initial concentration of 2,4-D

The influence of the initial concentration of 2,4-D was investigated with concentrations of 20ppm, 40ppm, and 60ppm for the 30%TiO_2/Fe-MCM 41 material. The obtained results were shown in Fig. 8.

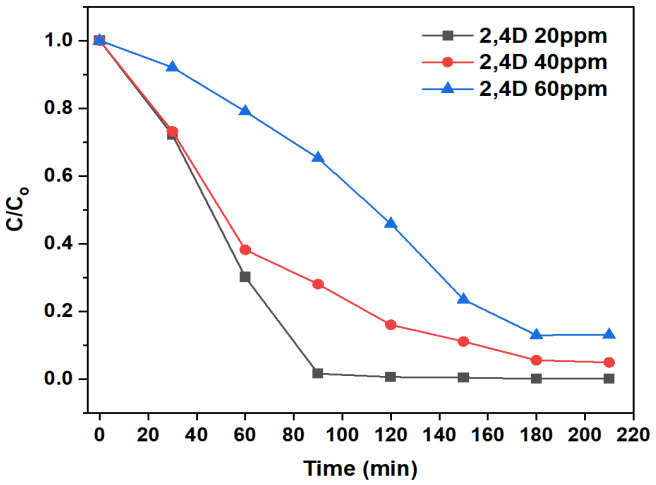

Fig. 8. The influence of the initial concentration of 2,4-D on the photodegradation over 30% TiO$_2$/Fe-MCM 41 material

The results showed that increasing illumination time significantly enhanced 2,4-D degradation across all initial concentrations. At 90 minutes, nearly complete degradation (99%, was achieved for a 20ppm solution. In contrast, efficiencies were lower for higher concentrations 65.19% at 40ppm and 34.75% at 60ppm.

After 210 minutes, 2,4-D at 20 ppm was almost fully degraded, and even at 40ppm, degradation reached about 97%. These results indicate that the 30% TiO_2/Fe-MCM-41 composite remains highly effective at treating 2,4-D solutions up to 40 ppm.

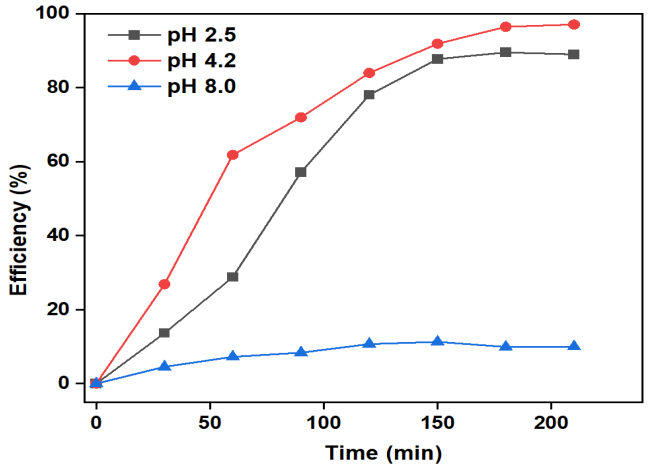

Fig. 9. The influence of pH solution on the photodegradation for 30% TiO_2/Fe-MCM 41 material

Effect of pH solution

To investigate the effect of pH on the degradation of 2,4-D, experiments were conducted at pH values of 2.5, 4.2, and 8.0, representing acidic and basic environments. The results indicated that 2,4-D degradation was more efficient under acidic conditions (Fig. 9). At pH 8.0, removal efficiency was low, with only about 10% degradation observed at an initial concentration of 40ppm. In contrast, at pH 4.2, the degradation efficiency improved markedly dropping from 40ppm to 15.27ppm (61.82%) after 60 minutes, and further down to 1.16ppm (over 97%) after 210 minutes. This can be attributed to the positively charged surface of the TiO_2-based photocatalyst in an acidic medium, which facilitates the migration of photogenerated electrons to the catalyst surface. This process promotes the formation of reactive radicals such as $O_2^{\bullet-}$ and $OH^{\bullet}$ in the aqueous phase, while also suppressing the recombination of photogenerated electron-hole pairs [19 - 21]. Additionally, since 2,4-D is a weak acid, it primarily exists in an anionic form within the pH range of 4.0. A relevant question arises as to whether the degradation efficiency of 2,4-D continues to increase at pH levels lower than 4.2, such as pH 2.5. To explore this, additional experiments were conducted at pH 2.5. However, the results showed a decline in degradation efficiency compared to pH 4.2. After 60 minutes, only 28.79% of 2,4-D was degraded (corresponding to 28.48ppm), and the degradation efficiency reached 89.3% (4.28ppm) after 210 minutes. This reduction in efficiency at pH 2.5 may be attributed to the extremely acidic environment, which could alter the surface charge of 2,4-D and reduce the electrostatic attraction between the pollutant and the photocatalyst, thereby hindering the degradation process.

Effect of free radicals in the photodegradation mechanism

To determine how these three free radicals contributed to the 2,4-D decomposition under light irradiation, three free radicals such as $O_2^{\bullet-}$, $^{\bullet}OH$, and photogenerated holes were examined. The radical scavengers used were ascorbic acid-AA (for $O_2^{\bullet-}$), tert-butyl alcohol (t-BuOH) (for $^{\bullet}OH$), and Na-EDTA (for photogenerated h^+ holes). Fig 10 displayed the effect of free radicals in the degradation mechanism of 2,4-D.

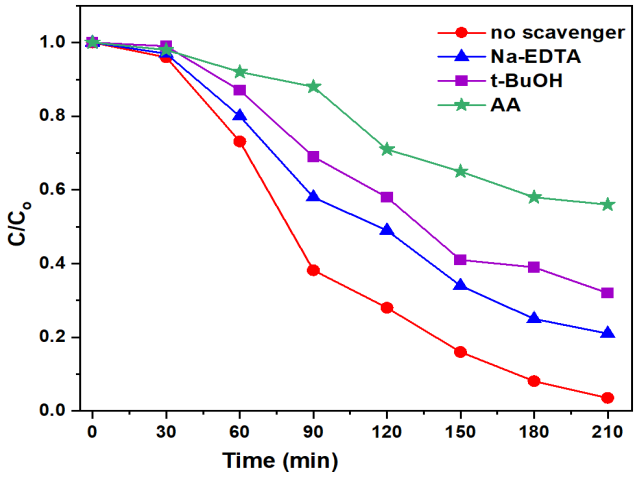

Fig. 10. Effect of free radicals in the 2,4-D photodegradation over 30%TiO_2/Fe-MCM 41 material

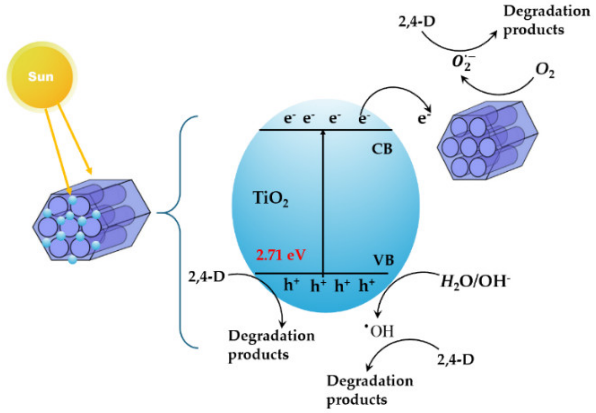

Fig. 11. The suggested photocatalytic mechanism for 30%TiO_2/Fe-MCM41 under light illumination

As shown in Fig. 10, the presence of radical scavengers such as ascorbic acid (AA), tert-butanol (t-BuOH), and Na-EDTA significantly reduced the 2,4-D degradation

efficiency. Without any scavengers, the removal efficiency reached approximately 97.01%. This indicates that reactive species - superoxide radicals ($O_2^{\bullet-}$), hydroxyl radicals ($^{\bullet}OH$), and photogenerated holes (h^+) are key contributors to 2,4-D photodegradation. Among the scavengers, AA had the strongest inhibitory effect, suggesting that $O_2^{\bullet-}$ plays a more dominant role in the photocatalytic process than $^{\bullet}OH$ and h^+.

A possible mechanism discussion

In the photocatalytic mechanism, the transfer of photoexcited e^- and h^+ depends on the valence band (VB) and conduction band (CB) potentials, and E_g. Their potentials were calculated by Eq (3, 4) [20, 21].

$$E_{VB} = \chi - E_e + 0.5E_g \quad (3)$$

$$E_{CB} = E_{VB} - E_g \quad (4)$$

Where $\chi \sim 5.81$eV for TiO_2; $E_e \sim 4.5$eV; E_g is the energy bandgap. The estimated VB and CB energies for 30%TiO_2/Fe-MCM 41 are 2.6eV and -0.02eV.

Based on the calculated values of CB and VB potentials, the charge separation, the photocatalytic mechanism may be proposed as in Fig. 11, consistent with the radical capturing experiment. The free radical formation and oxidative decomposition of 2,4-D under illuminated conditions were described by the reactions from (5) to (9).

$$TiO_2 + hv \rightarrow e^- + h^+ \quad (5)$$

$$TiO_2(e^-) + \text{Fe-MCM41} \rightarrow \text{Fe-MCM41}\ (e^-) + TiO_2 \quad (6)$$

$$\text{Fe-MCM41}\ (e^-) + O_2 \rightarrow O_2^{\bullet-} + \text{Fe-MCM41} \quad (7)$$

$$TiO_2\ (h^+) + {}^-OH \rightarrow {}^{\bullet}OH + TiO_2 \quad (8)$$

$$2,4\text{-D} + O_2^{\bullet-} / {}^{\bullet}OH / h^+ \rightarrow \text{Products} \quad (9)$$

Reusability studies

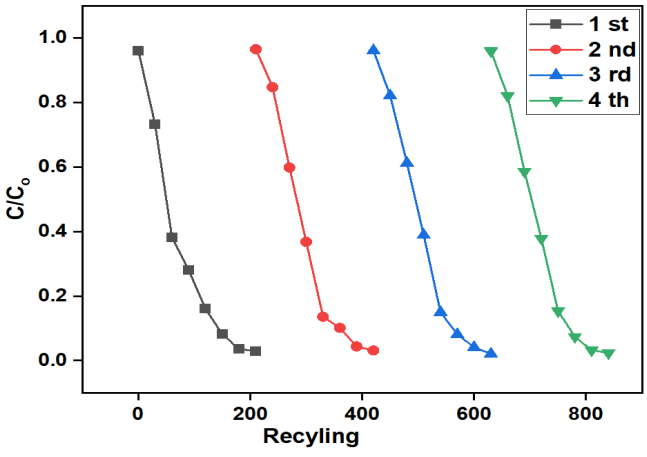

Fig. 12. Reusability studies of the 2,4-D treatment over 30%TiO2/Fe-MCM 41 material

The study on the recycling of 30%TiO_2/Fe-MCM-41 material in the decomposition of 2,4-D was carried out four times. The survey results were presented in Fig. 12.

The 2,4-D removal efficiency of 30%TiO_2/Fe-MCM-41 remained consistently above 97% after four consecutive cycles, with less than 5% variation between experiments. This demonstrates the material's excellent photocatalytic stability and effectiveness in degrading 2,4-D under light irradiation.

4. CONCLUSIONS

The 30%TiO_2/Fe-MCM-41 material was successfully synthesized and demonstrated high photocatalytic efficiency in degrading 2,4-D under light. At an initial concentration of 40ppm, pH 4.2 and 0.5g/L ratios of catalyst mass and volume, over 97% of 2,4-D was degraded after 210 minutes of illumination. The results highlight the crucial role of $O_2^{\bullet-}$, $^{\bullet}OH$ radicals, and photogenerated h^+ holes in the photocatalytic process. The material also showed excellent stability, maintaining consistent activity over four reuse cycles.

REFERENCES

[1]. Athanasekou C. P., Likodimos V., Falaras P., "Recent developments of TiO_2 photocatalysis involving advanced oxidation and reduction reactions in water," *J. Environ. Chem. Eng.*, 6, 7386-7494, 2018.

[2]. Rfan F., Tanveer M.U., Moiz M.A., "TiO_2 as an effective photocatalyst mechanisms, applications, and dopants: a review," *Eur. Phys. J. B,* 95, 184, 2022.

[3]. Malathi A., Madhavan J., Muthupandian A., Prabhakarn A., "A review on $BiVO_4$ photocatalyst: Activity enhancement methods for solar photocatalytic applications," *Appl. Catal. A: General,* 555, 47–74, 2018,

[4]. Li Z., Meng X., Zhang Z., "Recent development on MoS_2 -based photocatalysis: A review," J. Photochem. and Photobiology C: Photochemistry Reviews, 35, 39 - 55, 2018.

[5]. Chen L., Maigbay M. A., Li M., Qiu X., "Synthesis and modification strategies of g-C_3N_4 nanosheets for photocatalytic applications," *Adv. Powder Technol.*, 3, 1, 100150, 2024.

[6]. Guzmán C., Del Ángel G., Gómez R., Galindo-Hernández F., Ángeles-Chavez C., "Degradation of the herbicide 2,4-dichlorophenoxyacetic acid over Au/TiO_2-CeO_2 photocatalysts: Effect of the CeO_2 content on the photoactivity," *Catal. Today*, 166(1), 146-151, 2011.

[7]. Tang Y., Zhang G., Liu C., Luo S., Xu X., Chen L., Wang B., "Magnetic TiO_2-graphene composite as a high-performance and recyclable platform for efficient photocatalytic removal of herbicides from water," *J. Hazard. Mater.*, 252-253, 115-122, 2013.

[8]. Duong H. T. T., Duong M. T. P., Nguyen O. K., Le S. T., Dang L. V., Nguyen B. T., Do D. V., "Photocatalytic Activity of Ti-SBA-15/C_3N_4 for Degradation of 2,4-Dichlorophenoxyacetic Acid in Water under Visible Light," *J. Anal. Methods Chem*., ID 5531219, 10 pages, 2022.

[9]. Lim T.T., Yap P.S., Srinivasan, M., Fane A. G., "TiO_2/AC Composites for Synergistic Adsorption-Photocatalysis Processes: Present Challenges and Further Developments for Water Treatment and Reclamation," *Crit. Rev. Environ. Sci. Technol.,* 41(13), 1173-1230, 2011.

[10]. Chen W., Bao Y., Li X., Huang J., Xie J., Li L., "Role of Si-F groups in enhancing interfacial reaction of Fe-MCM-41 for pollutant removal with ozone," *J. Hazard. Mater.,* 393, 122387, 2020.

[11]. Guo Y., Chen B., Zhao Y., Yang T., "Fabrication of the magnetic mesoporous silica Fe-MCM-41-A as efficient adsorbent: performance, kinetics and mechanism," *Sci. Rep.,* 11, 2612, 2021.

[12]. Sönmez D.M., Gudovan D., Truşca R. Ficai D., Andronescu E., Vasile B.S., "Synthesis, characterization and testing of MCM-41/TiO_2 catalyst for organic dye degradation," *Dig. J. Nanomater. Biostruct.,* 10 (4), 1329-1341, 2015.

[13]. Trang N. T. T., Xuan M. T., Hoang N. V., Dong N. T., Linh P. T., Nguyet V. T., Nhiem N. T., Vinh T. Q., "Synthesis of mesoporous TiO_2-MCM-41 photocatalyst for quinolone antibiotics removal from aqueous solution," *Vietnam J. Chem*., 60, 589, 2022

[14]. Zanjanchi M. A., Golmojdeh H., Arvand M., "Enhanced adsorptive and photocatalytic achievements in removal of methylene blue by incorporating tungstophosphoric acid-TiO_2 into MCM-41," *J. Hazard. Mater.,* 169(1-3), 233-239, 2009.

[15]. Khieu D. Q., Quang D. T., Lam T. D., Phu N. H., Lee J. H., Kim J. S., "Fe-MCM-41 with highly ordered mesoporous structure and high Fe content: synthesis and application in heterogeneous catalytic wet oxidation of phenol," *J. Incl. Phenom. Macrocycl. Chem.,* 65(1-2), 73-81, 2009.

[16]. Sadjadi M. S., Farhadyar N., Zare K., "Synthesis of nanosize MCM-41 loaded with TiO_2 and study of its photocatalytic activity," *Superlattices Microstruct*., 46(1-2), 266-271, 2009.

[17]. Holzwarth U., Gibson N., "The Scherrer equation versus the "Debye-Scherrer equation", *Nat. Nanotechnol*., 6(9), 534 - 534, 2011.

[18]. Patrycja M., Michał P., Wojciech M., "How to Correctly Determine the Band Gap Energy of Modified Semiconductor Photocatalysts Based on UV–Vis Spectra," *J. Phys. Chem. Lett.,* 9 (23), 6814-6817, 2018.

[19]. Trang P. T. T., Tam T. T., Vien V., Lien N. H., "Application of MoS_2/reduced graphene oxide for photocatalytic degradation of rhodamine B in water environment," *IOP Conf. Ser.: Mater. Sci. Eng.,* 902, 012041, 2020.

[20]. Lan P. T., Hao N. H., Cam L. M., "Study on the Synthesis and Photocatalytic Performance of Modified TiO_2 Supported by g-C_3N_4 in the Degradation of 2,4-Dichlorophenoxyacetic Acid," *Chemistry Select*., 9, 12, e202305026, 2024.

[21]. Ruirui H., Guohong W., Hua T., Lingling S., Chang X., Deyan H., "Template-free preparation of macro/mesoporous g-C_3N_4/TiO_2 heterojunction photocatalysts with enhanced visible light photocatalytic activity," *Appl. Catal. B: Environ*., 187, 47-58, 2016.

[22]. Ghasemia S., Esfandiarb A., Rahman S. R., Habibi-Yangjehc A., Gholamia A. R., "Synthesis and characterization of TiO_2-graphene nanocomposites modified with noble metals as a photocatalyst for degradation of pollutants," *Appl. Catal. A: General,* 462 - 463, 82- 90, 2013.

THÔNG TIN TÁC GIẢ

Phùng Thị Lan[1], Nguyễn Thị Oanh[1], Đặng Đình Anh Tuấn[2], Nguyễn Thị Kim Giang[1]

[1]Khoa Hóa học, Trường Đại học Sư phạm Hà Nội

[2]Chuyên Vật lý, Trường THPT Chuyên Đại học Sư phạm Hà Nội